Mechanism of the OH-Initiated Oxidation of Hydroxyacetone over the Temperature Range 236−298 K†

Nadezhda I. Butkovskaya,* Nicolas Pouvesle, Alexander Kukui,‡ Yujing Mu,§ and Georges Le Bras

CNRS, Laboratoire de Combustion et Systèmes Réactifs, 1C Av. de la Recherche Scientifique, 45071 Orléans Cedex 2, France

Received: November 3, 2005; In Final Form: January 17, 2006

The mechanism of the gas-phase reaction of OH radicals with hydroxyacetone ($CH_3C(O)CH_2OH$) was studied at 200 Torr over the temperature range 236−298 K in a turbulent flow reactor coupled to a chemical ionization mass-spectrometer. The product yields and kinetics were measured in the presence of O_2 to simulate the atmospheric conditions. The major stable product at all temperatures is methylglyoxal. However, its yield decreases from 82% at 298 K to 49% at 236 K. Conversely, the yields of formic and acetic acids increase from about 8% to about 20%. Other observed products were formaldehyde, CO_2 and peroxy radicals HO_2 and $CH_3C(O)O_2$. A partial re-formation of OH radicals (by ∼10% at 298 K) was found in the OH + hydroxyacetone + O_2 chemical system along with a noticeable inverse secondary kinetic isotope effect ($k_{OH}/k_{OD} = 0.78 \pm 0.10$ at 298 K). The observed product yields are explained by the increasing role of the complex formed between the primary radical $CH_3C(O)CHOH$ and O_2 at low temperature. The rate constant of the reaction $CH_3C(O)CHOH + O_2 \rightarrow CH_3C(O)CHO + HO_2$ at 298 K, $(3.0 \pm 0.6) \times 10^{-12}$ cm^3 molecule^{-1} s^{-1}, was estimated by computer simulation of the concentration−time profiles of the $CH_3C(O)CHO$ product. The detailed mechanism of the OH-initiated oxidation of hydroxyacetone can help to better describe the atmospheric oxidation of isoprene, in particular, in the upper troposphere.

1. Introduction

Hydroxyacetone (HAC, $CH_3C(O)CH_2OH$) is produced in the atmosphere mainly from the OH-initiated oxidation of isoprene, the main non-methane hydrocarbon in the troposphere. HAC is a product of the OH reaction with methacrolein ($CH_2{=}C(CH_3)$-CHO), which is one of the primary carbonyl compounds formed in the isoprene oxidation.[1,2] Convectively lifted isoprene has been suggested as a potential source of HO_x in the upper troposphere (UT),[3,4] which influences the ozone budget. The assessment of the HO_x formation potential of isoprene in the UT requires knowledge of the detailed mechanism of the isoprene oxidation, in particular, the kinetics and mechanism of the title reaction at the low temperatures of the UT. The major removal process of HAC is the reaction with OH radicals, photolysis being found of minor importance.[5] The rate constant of this reaction was recently measured in the range of temperatures covering those of the UT.[6] However, the branching ratio of the OH + HAC reaction and the mechanism of further oxidation steps in air were not studied.

The structure−reactivity relationship of Kwok and Atkinson[7] predicts that the bulk of the reaction (91%) proceeds by abstraction of a secondary H-atom (1a), and the contributions from the two other possible abstraction pathways are 5% (1b) and 4% (1c):

$$OH + CH_3C(O)CH_2OH \rightarrow CH_3C(O)CHOH + H_2O \quad (1a)$$

$$\rightarrow CH_3C(O)CH_2O + H_2O \quad (1b)$$

$$\rightarrow CH_2C(O)CH_2OH + H_2O \quad (1c)$$

In air, the $CH_3C(O)CHOH$ radical from the main channel (1a) reacts with oxygen to give supposedly methylglyoxal (MGL) and HO_2:[5]

$$CH_3C(O)CHOH + O_2 \rightarrow CH_3C(O)CHO + HO_2 \quad (2)$$

Reaction 2 was studied by Jenkin et al.,[8] who determined a 100 ± 5% yield of HO_2 and suggested an equal yield of MGL. The primary radical from (1b) promptly decomposes to acetyl radical and formaldehyde as found in the study of the oxidation of acetone:[8]

$$CH_3C(O)CH_2O \rightarrow CH_3CO + CH_2O \quad (3)$$

Acetyl radical reacts with oxygen forming acetylperoxy radical (APR):

$$CH_3CO + O_2\ (+M) \rightarrow CH_3C(O)OO \quad (4)$$

The atmospheric transformations of APR are well defined,[9,10] leading to peroxy acetyl nitrate (PAN) in the presence of NO_x. The oxidation of the primary radical from (1c) has not been studied so far and the products of its reaction with oxygen are not known:

$$CH_2C(O)CH_2OH + O_2 \rightarrow \text{products} \quad (5)$$

† Part of the special issue "David M. Golden Festschrift".

* Corresponding author. E-mail: bout@cnrs-orleans.fr. Permanent address: Institute of Chemical Physics of the Russian Academy of Sciences, 117334 Moscow, Russian Federation.

‡ CNRS, Service d'Aéronomie, Paris.

§ Research Center for Eco-Environmental Sciences, Academia Sinica, Beijing 100085, China.

10.1021/jp056345r CCC: $33.50
Published on Web 03/10/2006

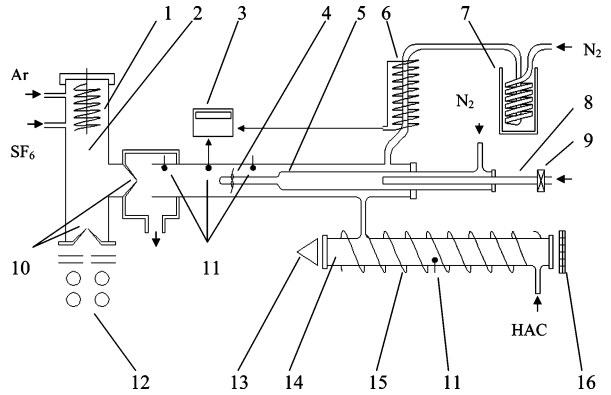

Figure 1. Experimental setup: 1, ion source; 2, ion molecule reactor; 3, temperature controller; 4, "turbulizer"; 5, injector; 6, resistance; 7, cooling bath; 8, discharge tube; 9, microwave discharge; 10, sampling cones; 11, temperature sensor; 12, mass analyzer; 13, UV lamp; 14, absorption cell; 15, resistance; 16, UV detector.

The aim of the present work was to determine the branching ratio for reaction 1 and the mechanisms of reactions 2 and 5 at temperatures relevant for the UT by direct detection of reaction products in the presence of molecular oxygen using chemical ionization mass spectrometry in the temperature range 236−298 K. In addition, the UV absorption spectra of HAC has been re-determined in support of measurements of HAC concentrations that were required in this study.

2. Experimental Section

2.1. Chemical Reactor. The experiments were conducted using a high-pressure turbulent flow reactor (TFR) coupled to chemical ionization mass-spectrometer (CIMS) The scheme of the experimental setup is presented in Figure 1. The reactor was operated at Reynolds number Re = 7300 and a pressure of 200 Torr with the typical flow velocity of N_2 carrier gas of 18 m/s. A detailed description of the experimental setup and validation of the flow conditions were presented in a previous work from this laboratory.[11]

A movable injector served as a pre-reactor to produce OH radicals in reactions

$$F + H_2O \rightarrow OH + HF \quad (6)$$

$$H + NO_2 \rightarrow OH + NO \quad (7)$$

with F- and H-atoms generated by a microwave discharge in the F_2/He or H_2/He gas mixtures in a quartz tube concentrically connected to the injector. To examine the products of the reaction of HAC with F-atoms, a F_2/He mixture was used without introduction of H_2O in the injector. Tank grade F_2 and H_2 (Alpha Gas 2) were used without further purification. NO_2 was obtained by keeping a mixture of NO with O_2 during 24 h followed by pumping out the oxygen through a liquid N_2 trap. After that NO_2 diluted in He (~1 and 12% mixtures) was stored in glass flasks. The maximal distance from the injector tip to the orifice of the inlet cone of the ion−molecule reactor was 50 cm, which corresponded to a reaction time *t* in the TFR of about 30 ms. The preliminary flow tests[11] showed that at Re > 2300 the minimal distance at which the turbulent mixing provided accurate measurements of the reaction rates was 3 cm. In the present study this distance corresponded to a reaction time of ~2 ms. Kinetic measurements in several chemical systems showed that the appearance of primary products at reaction time as short as 2 ms was in good agreement with the calculated time profiles.[11,12]

Hydroxyacetone (Fluka, >95%) was introduced into the reactor upstream of the tip of the movable injector along with a He flow (70 sccm) passing through the trap containing a liquid sample. The sample was additionally purified in several thaw and pump cycles. HAC concentration was measured on-line by UV absorption spectroscopy using a light at $\lambda = 254$ nm from a Hg lamp. The OH radicals signal was calibrated by measuring the consumption of NO_2 in reaction 7 by introducing small concentrations of NO_2 into the main reactor as previously described.[12] The concentration of F-atoms was determined by chemical titration in their fast reaction with acetaldehyde or methanol. The following compounds were used for calibration purposes: acetaldehyde (Fluka, 99.9%); methanol (99%); propyne (Sigma-Aldrich, >98%); acetic acid (Fluka, glacial 99.9%); formic acid (Riedel-deHaën, 98−100% extra pure). Their flow rates were measured by the drop of pressure in a calibrated volume using manometrically pre-prepared mixtures in He. The O_2 concentration in the reactor was determined mass-spectrometrically by flowing a known concentration of O_2 into the reactor.

2.2. CIMS Detection. Gas mixtures from the TFR were sampled through a Teflon cone into the ion−molecule reactor (IMR). The IMR was a stainless steel tube located perpendicular to the chemical reactor. The pressure of the Ar carrier gas in the IMR was about 1 Torr. The primary Ar^+ ions and electrons were generated in the ion source by a heated filament. SF_6 was continuously introduced into the IMR downstream of the ion source. The primary SF_6^- negative ions were produced by attachment of thermalized electrons to SF_6. Fragment ions, mainly F^- and SF_5^-, were also observed in the SF_6 spectrum, their intensity being about 3−5% of that of SF_6^-.

OH radicals and NO_2 were detected as OH^- (*m*/*e* 17) and NO_2^- (*m*/*e* 46) ions formed by electron transfer from SF_6^-.[13] HO_2 radicals were detected at *m*/*e* 140 using the known ion−molecule reaction:[14]

$$SF_6^- + HO_2 \rightarrow [SF_4 \cdot O_2]^- + \text{other products}$$

Acetylperoxy radicals, $CH_3C(O)OO$, could be detected at *m*/*e* 75 as $CH_3CO_3^-$ ions, as was previously determined.[15] CO_2 was detected as CO_3^- ions (*m*/*e* 60) using the ion−molecule reaction:[16]

$$O_3^- + CO_2 \rightarrow CO_3^- + O_2$$

where O_3^- ions were produced by adding a small quantity of ozone to the SF_6 flow:

$$SF_6^- + O_3 \rightarrow O_3^- + SF_6$$

HAC and other organic compounds were detected both in negative mode, using reactions with SF_6^- and fragment ions, and in positive mode, using proton-transfer reactions (PTR) from H_3O^+ ions and their water clusters. To produce H_3O^+ ions, H_2O vapor was flowed into the IMR downstream of the ion source along with SF_6. In the absence of reactants, the major positive ions observed in the IMR were H_3O^+ and their water clusters $H_3O^+ \cdot (H_2O)_n$, with $n = 1-3$. Using $H_3O^+(H_2O)_n$ ions, organic products with proton affinity (PA) greater than that of H_2O, 165 kcal mol^{-1}, can be detected by proton-transfer reactions:[13,17,18]

$$H_3O^+ \cdot (H_2O)_n + M \rightarrow MH^+ \cdot (H_2O)_m + (n - m + 1) \cdot H_2O \qquad m \le n$$

TABLE 1: Mass Numbers of Organic Molecules Observed in PTR Mode

molecule	PA[a]	mass	CH_3-CO^+	M_{-OH}^+	MH^+	$MH^+\cdot H_2O$	$MH^+\cdot (H_2O)_2$	$MH^+\cdot (H_2O)_3$
H_2O	165	18			19	37	55	73
CH_2O	170	30			31	49	67	
CH_3OH	180	32			33	51	69	
CH_3CCH	179	40			41	59	77	
CH_3CHO	184	44	43		45	63	81	
HCOOH	177	46			47	65	83	
CH_3COOH	187	60	43	43	61	79	97	
$CH_3C(O)CHO$		72	43		73	91	109	
$CH_3C(O)CH_2OH$		74	43	57	75	92	110	

[a] Proton affinity in kcal mol^{-1} from ref 18.

TABLE 2: Mass Numbers of Organic Molecules Observed in Negative Mode

molecule	mass	$(M_{-H})^-$	$(M_{-H})^-\cdot HF$	$(M_{-H})^-\cdot (HF)_2$
HCOOH	46	45	65	85
CH_3COOH	60	59	79	99
$CH_3C(O)CHO$	72	71	91	111
$CH_3C(O)CH_2OH$	74	73	93	113

Table 1 presents the compounds observed in the PTR regime in the present study.

In negative mode, spectra of HAC, formic and acetic acids exhibit a series of lines, which can be assigned to the products of the reactions with SF_6^- and/or F^-:

$$SF_6^- + RH \rightarrow R^- + SF_5 + HF$$

$$\rightarrow R^-(HF) + SF_5$$

$$F^- + RH \rightarrow R^- + HF$$

$$R^- + HF + M \rightarrow R^-\cdot(HF) + M$$

The $R^-(HF)_2$ clusters were observed in the spectra of formic and acetic acids as well. The corresponding mass numbers are given in Table 2. Weak signals at *m*/*e* 39 and 59 were observed in the formic acid spectrum, which were assigned to $F^-\cdot HF$ and $F^-\cdot(HF)_2$ ions formed in the IMR. For HAC, the observed *m*/*e* 59 peak can originate from $CH_3CO_2^-$ ion favored by a large electron affinity of the CH_3CO_2 radical (3.3 eV) and/or $HOCH_2CO^-$ ion. The HAC negative spectrum also contains weak lines at *m*/*e* 92 and 112 attributed to $C_3H_4O_2^-\cdot HF$ and $C_3H_4O_2^-\cdot(HF)_2$ ions. The negative spectrum of acetaldehyde consists of a single line at *m*/*e* 43 that can correspond to the CH_2CHO^- ion produced in the reaction with F^-.

2.3. Hydroxyacetone Absorption Cross-Section. In the present study, accurate measurement of HAC concentration was necessary to determine the product yields and kinetic isotope effects in reaction 1. Comparison of the HAC concentrations measured by absorption spectroscopy and by titration using a known concentration of F-atoms, showed a systematic underestimation of [HAC] by spectroscopic method applying a σ value at 254 nm from the only previous measurement of the HAC absorption cross-section in the 235−340 nm range.[5] To ascertain a cross section, we remeasured the UV absorption spectrum of HAC in the 240−360 nm range. The setup used for absorption measurements was described previously.[19] Briefly, a UV−visible spectrophotometer (Chromex 250IS) equipped with a 1800 grooves/mm grating and a 1024 element diode array detector (Princeton Instrument) was used. The output from a D_2 lamp was passed through a 100 cm long and 2.5 cm i.d. absorption cell and focused onto the entrance slit of the spectrometer. To reduce photodecomposition, a filter was used to cut off the UV light below 230 nm. The spectrum was measured by two methods. In the static method, the light intensity was measured when the cell was filled with a certain concentration of HAC, whereas in the so-called dynamic method it was measured when a fixed flow of HAC was passed through the cell at a fixed pressure. The UV spectra were obtained at eight pressures ranging from 1 to 2.5 Torr for the static method, and at four pressures ranging from 0.7 to 1.3 Torr for the dynamic method. In addition, measurements were performed at two temperatures to test the sensitivity of the cross-section to ambient conditions. The results are presented in Table 3. The standard deviation was less than 5% over the wavelengths between 250 nm and 300 nm, and larger than 10% at wavelength greater than 300 nm. The maximum absorption cross-section is around 267 nm, which is in agreement with the value of 266 nm reported by Orlando et al.[5] However, our maximum values were about 13% and 20% less than that of these authors, respectively for the dynamic and static methods (Figure 2). The $\sigma(254)$ values obtained are (in 10^{-20} cm^2 $molecule^{-1}$): 4.42 for the static method at 294 K, 4.31 for the static method at 328 K and 3.82 for dynamic method at 328 K. We see that the change with temperature is within the error limits of the measurements. This values can be compared with $\sigma(254) = 5.54 \times 10^{-20}$ cm^2 $molecule^{-1}$ reported by Orlando et al. and measured with an uncertainty of about 20%. A value of $\sigma(254) = 4.42 \times 10^{-20}$ cm^2 $molecule^{-1}$, which corresponded well to the results of chemical titration, was used in the present study.

TABLE 3: UV Absorption Cross Sections for Hydroxyacetone[a]

λ (nm)	static 294 K	dynamic 328 K	λ (nm)	static 294 K	dynamic 328 K	λ (nm)	static 294 K	dynamic 328 K
240	2.09		277	4.70	5.08	314	0.187	0.259
241	2.26		278	4.56	4.95	315	0.160	0.245
242	2.43		279	4.41	4.77	316	0.130	0.238
243	2.60		280	4.24	4.62	317	0.0954	0.227
244	2.75		281	4.05	4.43	318	0.0765	0.200
245	2.93		282	3.87	4.26	319	0.0737	0.177
246	3.13		283	3.70	4.09	320	0.143	0.164
247	3.31		284	3.51	3.92	321	0.138	0.149
248	3.48		285	3.32	3.78	322	0.130	0.139
249	3.65		286	3.13	3.60	323	0.123	0.142
250	3.82	2.79	287	2.93	3.40	324	0.111	0.136
251	4.01	3.06	288	2.71	3.18	325	0.0980	0.130
252	4.16	3.34	289	2.48	2.94	326	0.0865	0.132
253	4.30	3.58	290	2.28	2.73	327	0.0764	0.120
254	4.42	3.82	291	2.08	2.54	328	0.0728	0.106
255	4.56	4.08	292	1.91	2.37	329	0.0721	0.0986
256	4.72	4.39	293	1.74	2.19	330	0.0706	0.0953
257	4.86	4.67	294	1.58	2.03	331	0.0697	0.127
258	4.99	4.92	295	1.43	1.85	332	0.0663	0.127
259	5.08	5.11	296	1.28	1.67	333	0.0591	0.116
260	5.16	5.30	297	1.15	1.51	334	0.0547	0.113
261	5.23	5.45	298	1.02	1.34	335	0.0566	0.106
262	5.31	5.57	299	0.919	1.20	336	0.0647	0.101
263	5.36	5.68	300	0.829	1.07	337	0.0656	0.0985
264	5.39	5.75	301	0.787	0.974	338	0.0713	0.0994
265	5.40	5.79	302	0.700	0.877	339	0.0767	0.0963
266	5.43	5.85	303	0.621	0.772	340	0.0852	0.106
267	5.43	5.86	304	0.553	0.685	341	0.0935	0.110
268	5.43	5.85	305	0.501	0.617	342	0.0965	0.113
269	5.41	5.82	306	0.460	0.553	343	0.0999	0.121
270	5.35	5.76	307	0.417	0.485	344	0.103	0.129
271	5.26	5.59	308	0.374	0.430	345	0.102	0.138
272	5.22	5.58	309	0.334	0.383	346	0.0998	0.137
273	5.14	5.49	310	0.294	0.348	347	0.0981	0.137
274	5.03	5.39	311	0.257	0.312	348	0.0945	0.140
275	4.93	5.28	312	0.223	0.289	349	0.0921	0.132
276	4.83	5.19	313	0.211	0.263	350	0.0903	0.134

[a] σ (10^{-20} cm^2 $molecule^{-1}$).

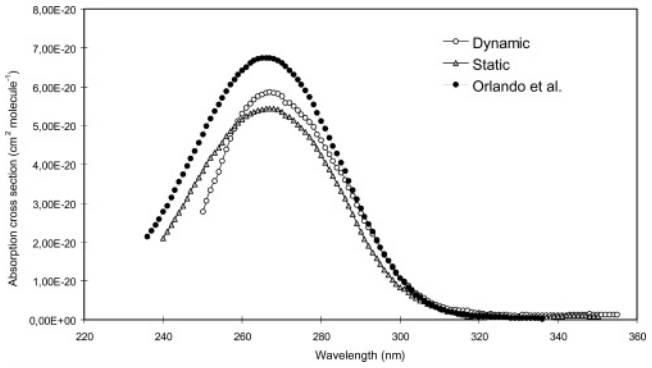

Figure 2. Absorption cross-sections for hydroxyactone measured using dynamic (328 K) and static (294 K) methods. The spectrum from Orlando et al.[5] at 298 K is shown for comparison.

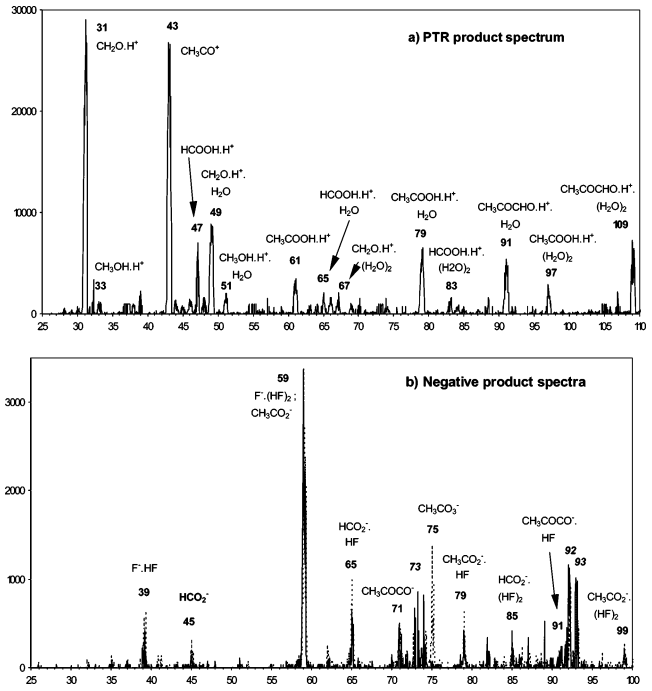

Figure 3. (a) PTR product spectrum from the F + HAC reaction. (b) Product spectra in negative registration regime from the F + HAC reaction (dotted) and OH + HAC reaction (solid). The observed peaks were assigned using Tables 1 and 2. Intensities are in counts per second (cps).

3. Results and Discussion

3.1. Product Spectra. The reaction of HAC with F-atoms was used to monitor product mass spectra. This reaction gives presumably the same products as reaction 1 but with larger branching ratios for the channels (1b) and (1c) that allows more reliable detection of the products from these minor channels. In addition, in our experiments it is easier to generate larger concentrations of F-atoms than OH radicals for qualitative observations. Figure 3 presents mass spectra acquired from F + HAC + O_2 reaction in PTR (a) and in negative (b) regimes at $T = 298$ K. A negative spectrum from OH + HAC + O_2 reaction is also shown for comparison. The concentrations were [HAC] = 1×10^{13}, [O_2] = 1×10^{16}, [F]$_o$ = 6×10^{11} and [OH]$_o$ = 4×10^{11} molecule cm^{-3}. These spectra present a difference between the discharge on and discharge off measurements. The negative spectra are normalized by the maximum peak intensity at *m*/*e* 59. The following products can be determined according to Tables 1 and 2: formaldehyde (PTR peaks 31/49/67), acetic acid (PTR peaks 43, 61/79/97 and negative series 59/79/99), formic acid (PTR peaks 47/65/83 and negative peaks 39, 45/65/85), methanol (PTR peaks 33/51/69) and MGL (PTR peaks 43, 91/109; peak 73 coincides with the heaviest observed $H_3O^+(H_2O)_3$ cluster ion). The peaks at *m*/*e* 59, 71 and 91 in negative mode can be attributed to MGL. The assignment of the peaks 92 and 93 is not clear, as these peaks (and that at *m*/*e* 73) belong to the spectrum of HAC and can be a result of subtraction of the large intensities due to the reactant. The peak at *m*/*e* 75 in negative mode corresponds to the $CH_3C(O)OO^-$ ion formed in reaction 4.[15] Also, the peak at *m*/*e* 140 belonging to the HO_2 radical was observed in negative mode (not shown in the spectrum). Thus, the observed spectra confirmed production of MGL and HO_2 from (1a), and formaldehyde and CH_3CO from (1b). In addition, they show evidence for formation of acetic and formic acids. The difference between the negative spectra from the F + HAC + O_2 reaction and that from the OH + HAC + O_2 reaction was the strong decrease of the acetylperoxy radical peak at *m*/*e* 75; the relative intensities of the MGL and acids peaks remained unchanged. This indicates that acetic and formic acids originate mainly from the major channel (1a). The yields of the detected products determined at different temperatures are presented in the next section.

3.2. Product Yields in the OH + $CH_3C(O)CH_2OH$ + O_2 System. *(a) CO_2.* CO_2 signal intensity from the OH + HAC + O_2 reaction was measured using the H + NO_2 reaction as a source of OH radicals and not F + H_2O, because water significantly reduced the detection sensitivity to CO_2. CO_2 calibration was accomplished using a measured flow of a 3% CO_2/He mixture. During the calibration, the same HAC and O_2 concentrations were maintained in the reactor as during the measurement of the CO_2 signal from the reaction. Unfortunately, the signal of CO_2 at *m*/*e* 60 overlapped with a minor peak from HAC and was sufficiently stable only at room temperature. First, OH kinetics were monitored in the absence and in the presence of HAC and O_2 with [HAC] = 2.6×10^{13} and [OH]$_0$ = 7.2×10^{11} molecule cm^{-3}. This allowed a determination of the amount of OH consumed by HAC: $\Delta[OH]_r = ([OH]_0 - [OH]_{fr}) \ln([OH]_{fr}/[OH]_f)/\ln([OH]_{fr}/[OH]_0) = 4.5 \times 10^{11}$ molecule cm^{-3}, where [OH]$_f$ and [OH]$_{fr}$ are the final OH concentration at reaction time t without and with HAC in the reactor, respectively (see ref 20 for derivation of this expression). With account of OH regeneration (vide infra), the consumed OH concentration becomes $\Delta[OH]_r = 4.9 \times 10^{11}$ molecule cm^{-3}. The CO_2 signal from the reaction was measured at $t = 29$ ms with [O_2] = 1.2×10^{15} molecule cm^{-3}. The average CO_2 product concentration was $\Delta[CO_2] = (5.7 \pm 1.2) \times 10^{10}$ molecule cm^{-3}. This value was obtained from sixteen discharge on−off measurements of the signal. The average yield is $\Delta[CO_2]/\Delta[OH]_r = 11.7 \pm 2.8\%$.

(b) $CH_3C(O)CHO$. The yield of MGL from the successive reactions 1a and 2

$$OH + CH_3C(O)CH_2OH \rightarrow CH_3C(O)CHOH + H_2O \quad (1a)$$

$$CH_3C(O)CHOH + O_2 \rightarrow CH_3C(O)CHO + HO_2 \quad (2)$$

was determined by calibrating MGL using the OH reaction with propyne in excess of O_2 with the known MGL yield of 53 ± 3%:[21]

$$OH + CH_3CCH + O_2 \rightarrow CH_3C(O)CHO + \text{other products} \quad (8)$$

There are two available values for the rate constant of the OH + CH_3CCH reaction at 298 K: 5.7×10^{-12} [21] and 2.9×10^{-12}

TABLE 4: Measurements of the Yields (in %) of Methylglyoxal, Φ(MGL), and Formaldehyde, Φ(CH_2O), in the OH + $CH_3C(O)CH_2OH$ + O_2 System (PTR Regime)[a]

T (K)	$\Delta^{Pr}I_{109}$	ΔI_{109}	Δ[MGL]	Φ(MGL) *m/e* 109	ΔI_{31}	Δ[CH_2O] *m/e* 31	ΔI_{49}	Δ[CH_2O] *m/e* 49	Φ(CH_2O)
				[CH_3CCH] = 240; Δ[CH_3CCH] = 3.81; [HAC] = 330; $\Delta[OH]_r$ = 3.93					
298	2462 ± 82	3871 ± 347	3.15	80.1 ± 11.1	487 ± 109	0.38	177 ± 28	0.35	9.2 ± 2.0
263		3567 ± 315	2.90	73.8 ± 10.1	440 ± 68	0.34	199 ± 23	0.39	9.4 ± 1.7
237		2374 ± 443	1.93	49.1 ± 10.5	546 ± 78	0.42	251 ± 53	0.50	11.8 ± 2.4
				[CH_3CCH] = 234; Δ[CH_3CCH] = 1.65; [HAC] = 287; Δ[HAC] = 1.69					
298	209 ± 10	338 ± 32	1.41	83.6 ± 11.0	151 ± 18	0.19	82 ± 11	0.17	10.7 ± 1.7
273		318 ± 28	1.28	76.0 ± 9.8	152 ± 12	0.20	85 ± 7	0.17	11.0 ± 1.5
253		261 ± 28	1.09	64.7 ± 9.2	140 ± 24	0.18	106 ± 25	0.22	11.8 ± 2.4
236	225 ± 18	195 ± 35	0.82	48.7 ± 9.9	174 ± 24	0.22	114 ± 24	0.23	13.4 ± 2.4

[a] Concentrations are in 10^{11} molecule cm^{-3}. $\Delta^{Pr}I_M$ and ΔI_M denote a change of the signal (in cps) at *m/e* M with switching on the discharge in the propyne and hydroxyacetone reactions, respectively. See text for description of the OH + CH_3CCH + O_2 chemical system used for calibration of MGL and F + CH_3OH + O_2 system used for calibration of CH_2O.

cm^3 $molecule^{-1}$ s^{-1}.[23] Taking the average value of 4.3×10^{-12} cm^3 $molecule^{-1}$ s^{-1}, the characteristic reaction time for OH + CH_3CCH reaction is about 10 ms. The experiments were conducted at $t = 30$ ms with [CH_3CCH] ≥ 2.3×10^{13} and [O_2] ≈ 2×10^{16} molecule cm^{-3}, which ensured completion of reaction 8. The mechanism suggested for the global reaction 8 included regeneration of OH,[21,22] which is why the sensitivity to MGL was found from the consumption of propyne in reaction 8: Δ[MGL] = 0.53·Δ[CH_3CCH]. Two experiments were carried out to quantify the MGL signal from the OH + HAC + O_2 system. In the first one, an accurate calibration of the OH signal was made, the initial OH concentration from the F + H_2O source was determined to be 4.8×10^{11} molecule cm^{-3}. The MGL yield from reactions 1 and 2 was determined taking a ratio of the formed MGL to the OH reacted with HAC, Δ[MGL]/$\Delta[OH]_r$, with $\Delta[OH]_r$ determined as in the previous paragraph from the OH known rate constants of the reaction and wall loss. The consumption of propyne in reaction 8 measured at *m/e* 41 in the PTR regime was $(3.8 \pm 0.3) \times 10^{11}$ molecule cm^{-3}; the error limit is the standard deviation of the six discharge on−off signal measurements. The signal of MGL in PTR regime at *m/e* 109 from reaction 8 was 2462 ± 82 cps, giving a sensitivity of 8.13×10^7 molecule cm^{-3}/cps. Then, propyne was changed for hydroxyacetone ([HAC] = 3.3×10^{13} molecule cm^{-3}), keeping the same OH and oxygen concentrations and the signal at *m/e* 109 from the reaction with HAC was measured to be 3871 ± 347 cps. The OH consumption by HAC in reaction 1 was estimated to be $\Delta[OH]_r = (3.9 \pm 0.4) \times 10^{11}$ molecule cm^{-3} giving the MGL yield of 80% at 298 K (see Table 4). The measurements of the signal intensity of MGL from reactions 1 and 2 in the PTR regime were repeated at T = 263 and 237 K and also presented in Table 4. The signal of HAC at *m/e* 75 was monitored during the cooling of the reactor. It was stable down to $T \sim 230$ K; at lower temperature an abrupt drop of intensity was observed. For other compounds, such as NO_2, CH_3CHO, CH_3COOH, and HNO_3, we did not observe a change of signal intensity in the 298−223 K range. However, this behavior set the lower temperature limit of ∼233 K for the experiments with HAC.

In the second experiment, MGL was calibrated in the same manner, but the MGL yield in the hydroxyacetone system was determined as Δ[MGL]/Δ[HAC]. Reaction occurred with [HAC] = 2.9×10^{13} and [O_2] = 2.7×10^{16} molecule cm^{-3}. During the cooling, the MGL and HAC signals were monitored. The HAC consumption measured with an accuracy of about 10% was 1.64, 1.58, 1.72 and 1.80×10^{11} molecule cm^{-3} at T = 298, 273, 253 and 236 K, respectively. As the change did not exceed the error limits, a mean value of $(1.69 \pm 0.08) \times 10^{11}$ molecule cm^{-3} was used for calculation of the MGL yield for all temperatures. The results are presented in Table 4. The average $CH_3C(O)CHO$ yield is about 82% at room temperature and drops noticeably with lowering temperature to about 49% at 237 K, indicating formation of other products.

(c) CH_2O. The signal of formaldehyde was monitored at *m/e* 31 and 49 in PTR regime simultaneously with the measurements of MGL yield described above. Calibration of formaldehyde was made using the reaction of F-atoms with methanol, which gives a 100% yield of formaldehyde in a large excess of O_2:

$$F + CH_3OH \rightarrow CH_2OH + HF \quad 41\% \qquad (9a)$$

$$\rightarrow CH_3O + HF \quad 57\% \qquad (9b)$$

$$CH_2OH + O_2 \rightarrow CH_2O + HO_2 \qquad (10)$$

$$CH_3O + O_2 \rightarrow CH_2O + HO_2 \qquad (11)$$

The branching ratio for reaction 9 is k_{9a}:k_{9b} = 41:57.[24] Reaction 10 is relatively fast, $k_{10} = 6 \times 10^{-12}$ cm^{-3} $molecule^{-1}$ s^{-1}, whereas reaction 11 with $k_{11} = 2 \times 10^{-15}$ cm^{-3} $molecule^{-1}$ s^{-1} needed [O_2] > 4×10^{16} molecule cm^{-3} for completion. Initial concentration of F-atoms was determined by chemical titration by CH_3OH. The CH_2O yield was determined as Δ[CH_2O]/$\Delta[OH]_r$ in the first experiment and as Δ[CH_2O]/Δ[HAC] in the second experiment (the same as for MGL measurements). The measured concentrations and the yields obtained at different temperatures are given in Table 4.

(d) CH_3COOH and HCOOH. The yields of acetic and formic acids were determined from signal detection in negative mode, monitoring CH_3COOH at *m/e* 79 and 99, and HCOOH at *m/e* 65. The reaction time was t = 28 ms, and concentrations were [HAC] = 2.64×10^{13}, $[OH]_0 = 3.40 \times 10^{11}$ and [O_2] = 1.7×10^{16} molecule cm^{-3}. The calculated consumption of OH radicals by HAC was 3.1×10^{11} molecule cm^{-3}, whereas the measured HAC consumption was somewhat higher, 4.4×10^{11} molecule cm^{-3}. The signals were calibrated using pre-prepared 1.5% mixtures of CH_3COOH and HCOOH in He. The calibration was carried out with the same HAC and O_2 concentrations in the reactor as those used in the course of the reaction. The results of the measurements are presented in Table 5. Two sets of the obtained yields correspond to Δ[acid]/$\Delta[OH]_r$ and Δ[acid]/Δ[HAC]. The last column presents an average value. For acetic acid, averaging was also done for the two measured signals. From Table 5 one can see that the yields of formic and acetic acids are very similar and that they noticeably increase with the decrease of temperature.

(e) HO_2 and $CH_3C(O)OO$. To measure the yields of radical products, proper kinetic conditions must be chosen to minimize

TABLE 5: Measurements of the Yields (in %) of Formic Acid, Φ(FA), and Acetic Acid, Φ(AA), in the OH + $CH_3C(O)CH_2OH$ + O_2 Chemical System (Negative Mode)[a]

T (K)	Δ[FA] *m/e* 65	Φ(FA)[b]	Φ(FA)[c]	Φ(FA)[d] *m/e* 65	Δ[AA] *m/e* 79	Δ[AA] *m/e* 99	Φ(AA)[d] *m/e* 79	Φ(AA)[d] *m/e*99	Φ(AA)[e]
				$[OH]_0 = 3.40$; [HAC] = 264; $\Delta[HAC] = 4.42$; $\Delta[OH]_r = 3.06$;					
295	0.249	8.14	5.82	7.0 ± 1.2	0.237	0.316	6.58	8.75	7.7 ± 1.8
273	0.416	13.6	9.73	11.7 ± 2.0	0.356	0.406	9.34	10.6	10.0 ± 2.4
253	0.614	20.1	14.3	17.2 ± 2.9	0.487	0.489	12.1	12.2	12.2 ± 2.2
236	0.805	26.3	18.8	22.6 ± 3.7	0.581	0.634	18.1	19.7	18.9 ± 2.6

[a] Concentration are in 10^{11} molecule cm^{-3}. [b] $\Delta[FA]/\Delta[OH]_r$; [c] $\Delta[FA]/\Delta[HAC]$; [d] Average values; [e] Average for two formic acid masses.

TABLE 6: Measurements of the HO_2 and $CH_3C(O)OO$ Yields (in %) in the OH + $CH_3C(O)CH_2OH$ + O_2 Chemical System at 298 K[a]

[HAC]	$[O_2]$	$[OH]_0$	$[OH]_r$	ΔI_{140}	$\Delta[HO_2]$	$\Phi(HO_2)$	ΔI_{75}	Δ[APR][b]	Φ(APR)[b]
450	2.4×10^4	8.3	5.2	653 ± 50	4.3	82 ± 13	408 ± 20	0.13	2.5 ± 0.7
400	1.2×10^4	2.4	1.9	175 ± 15	1.7	88 ± 13	46 ± 8	0.055	2.9 ± 0.9
295	2.5×10^4	6.5	2.4	402 ± 20	2.1	86 ± 10			

[a] Concentrations are in 10^{11} molecule cm^{-3}. [b] APR denotes acetylperoxy radical.

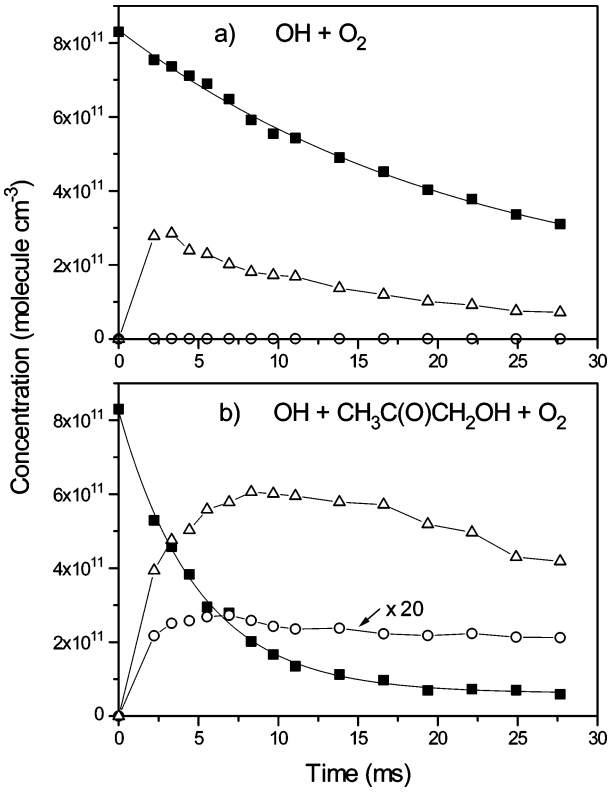

Figure 4. Concentration-time profiles of OH (■), HO_2 (△) and $CH_3C(O)OO$ (○) radicals in the absence of HAC (a) and with [HAC] = 4.2×10^{13} molecule cm^{-3} (b).

their losses. Figure 4b shows the temporal dependence of HO_2 and $CH_3C(O)OO$ radical signals at $[O_2] = 2.4 \times 10^{15}$ and [HAC] = 4.2×10^{13} molecule cm^{-3}. Calibration of HO_2 was made using its reaction with NO, converting HO_2 to NO_2. Formation of HO_2 in the absence of HAC is caused by the reaction of O_2 with H-atoms produced in the discharge from water impurities and varied from experiment to experiment. With the O_2 concentration used, this reaction is complete within 1 ms and the observed HO_2 decay is due to reaction with OH, self-reaction and wall loss. Reaction of H-atoms with added HAC cannot compete with reaction with O_2; hence, the HO_2 profile from reaction of HAC with OH in the presence of O_2 corresponded to the difference between the profiles in the presence and in the absence of HAC. The HO_2 yields were calculated from the difference in HO_2 signal intensities at $t \approx 8$ ms for which secondary reactions and wall losses were not important. Table 6 presents the conditions and results of three similar measurements of $\Phi(HO_2) = \Delta[HO_2]/\Delta[OH]_r$ done at 298 K. The obtained average yield is 85 ± 9%.

Acetylperoxy radicals (APR) formed from successive reactions 1b and 4 were quantified by their signal from the fast F + acetaldehyde reaction giving 65% of CH_3CO radicals,[25] 83% of which being converted to APR in the presence of O_2:[10]

$$F + CH_3CHO \rightarrow CH_3CO + HF \quad 65\% \quad (12a)$$

$$\rightarrow CH_2CHO + HF \quad 35\% \quad (12b)$$

$$CH_3CO + O_2(+M) \rightarrow CH_3C(O)OO \quad 83\% \quad (4a)$$

$$\rightarrow OH + \text{other products} \quad 17\% \quad (4b)$$

Special care should be taken to avoid possible influence of the $OOCH_2CHO$ radical formed in reaction 13a, which has the same mass as APR:

$$CH_2CHO + O_2 \rightarrow OOCH_2CHO \quad (13a)$$

$$\rightarrow OH + \text{other products} \quad (13b)$$

The rate constants are $k_4 = 4.1 \times 10^{-12}$ and $k_{13} = 1.9 \times 10^{-13}$ cm^3 $molecule^{-1}$ s^{-1} [26] and the concentration of O_2 during the calibration was about 1×10^{14} molecule cm^{-3}, so that reaction of the vinoxy radical with O_2 could not noticeably contribute to the signal at *m/e* 75, whereas acetyl radicals were efficiently transformed into the peroxy form. For example, to calibrate the signal shown in Figure 4, reaction with acetaldehyde was held with $[CH_3CHO] = 3.4 \times 10^{12}$, $[O_2] = 1.2 \times 10^{14}$ and $[F]_o = (4.4 \pm 0.2) \times 10^{11}$ molecule cm^{-3} at $t = 16$ ms. Fluorine atoms were titrated by acetaldehyde. The APR signal during the calibration was $\Delta I_{75} = 7415 \pm 70$ cps, and the obtained sensitivity $s(APR) = [F]\cdot(k_{12a}/k_{12})\cdot(k_{4a}/k_4)/\Delta I_{75} = (3.2 \pm 0.4) \times 10^7$ molecule cm^{-3} cps^{-1}. The signal observed from the OH reaction with HAC, $\Delta I_{75} = 408$ cps, corresponded to $\Delta[APR] = 1.3 \times 10^{10}$ molecule cm^{-3}, which gives $\Phi(APR) = \Delta[APR]/\Delta[OH]_r = 2.4 \pm 0.7\%$. This result and the one from another experiment are presented in Table 6. The obtained yields for all the products are summarized in Table 7.

3.3. Rate Constant of the Methylglyoxal Forming Reaction. The rate constant of the reaction of the $CH_3C(O)CHOH$ radical with O_2 (2a) was estimated from numerical simulation of the kinetic profiles of methylglyoxal formation in the F + HAC + O_2 system at different concentrations of oxygen.

TABLE 7: Summary of the Product Yields (in %) in the OH + Hydroxyacetone + O_2 System

T (K)	$CH_3C(O)CHO$	CH_2O	HCOOH	CH_3COOH	CO_2	HO_2	$CH_3C(O)O_2$	OH
298	82 ± 11	10 ± 2	7 ± 2	8 ± 2	12 ± 3	85 ± 12	3 ± 1	10 ± 3
273	76 ± 10	11 ± 2	12 ± 2	10 ± 2				14 ± 3
263	74 ± 10	9 ± 2						18 ± 4
253	65 ± 9	12 ± 2	17 ± 3	12 ± 2				21 ± 3
236	49 ± 10	13 ± 2	23 ± 4	19 ± 3				25 ± 5

TABLE 8: Scheme of the Reactions Used to Model the OD (OH) + HA + O_2 Chemical System in the TFR

N^a	k^b	reaction	N^a	k^b	reaction
14a	100	F + HAC → $CH_3COCHOH$ + HF	17	15	$CH_3C(O)OO + CH_3C(O)OO \rightarrow 2CH_3 + 2CO_2 + O_2$
14b	40	F + HAC → CH_2COCH_2OH + HF		11.4	$CH_3C(O)OO + HO_2 \rightarrow CH_3C(O)OOH + O_2$
14c	40	F + HAC → $CH_3CO + CH_2O$ + HF		40	$CH_3COCHOH + HO_2 \rightarrow$ products
1Da	3.8	OD + HAC → $CH_3COCHOH$ + HOD		13.2	OH(OD) + $CH_3COCHO \rightarrow CH_3CO + CO + H_2O$(HOD)
1Db	0.14	OD + HAC → $CH_3CO + CH_2O$ + HOD		0.34	$H + O_2(+M) \rightarrow HO_2$
1Dc	0.14	OD + HAC → CH_2COCH_2OH + HOD		80	$H + HO_2 \rightarrow OH + OH$
1a	2.9	OH + HAC → $CH_3COCHOH + H_2O$		2.1	$HO_2 + HO_2 \rightarrow H_2O_2 + O_2$
1b	0.11	OH + HAC → $CH_3CO + CH_2O + H_2O$		110	OH(OD)+ $HO_2 \rightarrow H_2O$(HOD) + O_2
1c	0.11	OH + HAC → $CH_2COCH_2OH + H_2O$		4.4	$OH + OH(+M) \rightarrow H_2O_2$
2a	2.8[d]	$CH_3COCHOH + O_2 \rightarrow CH_3COCHO + HO_2$		18[c]	OH(OD) → loss
2b	0.11[d]	$CH_3COCHOH + O_2 \rightarrow HCOOH + OH + CH_2CO$		12[c]	HO_2 → loss
2b′	0.14[d]	$CH_3COCHOH + O_2 \rightarrow HCOOH + CH_3 + CO_2$	7	140	$H + NO_2 \rightarrow OH + NO$
2c	0.11[d]	$CH_3COCHOH + O_2 \rightarrow CH_3COOH + OH + CO$		6.4	OH(OD) + $NO_2(+M) \rightarrow HNO_3(DNO_3)$
2c′	0.14[d]	$CH_3COCHOH + O_2 \rightarrow CH_3COOH + H + CO_2$		3	OH(OD) + NO(+M) → HONO(DONO)
4a	3.4	$CH_3CO + O_2 \rightarrow CH_3C(O)OO$	18	8.5	$HO_2 + NO \rightarrow OH + NO_2$
4b	0.7	$CH_3CO + O_2 \rightarrow CH_2O + OH + CO$		1	$CH_3 + O_2(+M) \rightarrow CH_3O_2$
5b	0.1[e]	$CH_2COCH_2OH + O_2 \rightarrow 2CH_2O + CO + OH$		30	$CH_3 + HO_2 \rightarrow CH_3O + OH$
5d	0.1[e]	$CH_2COCH_2OH + O_2 \rightarrow CH_2O + CH_2OH + CO_2$		120	$CH_3 + OH(+M) \rightarrow CH_3OH$
15	50	$CH_3C(O)OO$ + OH(OD) → $CH_3 + CO_2 + HO_2(DO_2)$		9.6	$CH_2OH + O_2 \rightarrow CH_2O + HO_2$
16	21	$CH_3C(O)OO + NO \rightarrow CH_3 + CO_2 + NO_2$			

[a] Number in the text. [b] Rate constants (in units of 10^{-12} cm^3 molecule^{-1} s^{-1}) were taken from the NIST kinetic database[27] except the specified cases: [c] This work; [d] Fitted value, [e] Analogy to $CH_2CHO + O_2$ reaction. Rate constants for third body reactions are for 200 Torr.

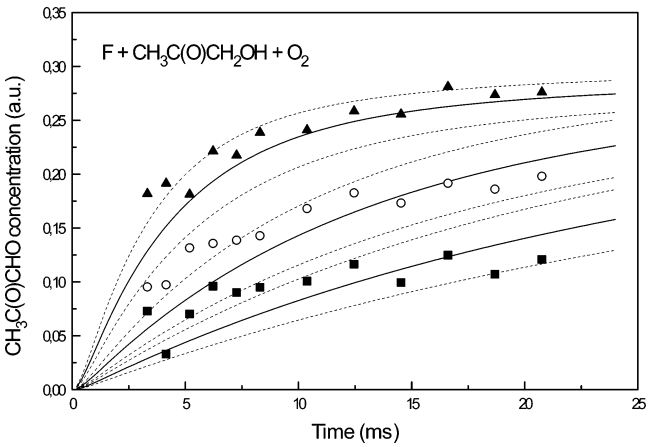

Figure 5. Methylglyoxal time profiles in the F + HAC + O_2 reaction at different O_2 concentrations: $[O_2] = 1.4 \times 10^{13}$ (■), 2.8×10^{13} (○) and 6.5×10^{13} (▲) molecule cm^{-3}. Initial concentrations were [HAC] $= 1.5 \times 10^{13}$ and [F] $= 5.4 \times 10^{11}$ molecule cm^{-3}.

Reaction with F-atoms as a source of $CH_3C(O)CHOH$ radicals was preferred because it is expected to be faster than reaction with OH, making it easier to investigate secondary oxidation processes:

$$F + CH_3C(O)CH_2OH \rightarrow CH_3C(O)CHOH + HF \quad (14)$$

$$CH_3C(O)CHOH + O_2 \rightarrow CH_3C(O)CHO + HO_2 \quad (2a)$$

Figure 5 presents the MGL formation curves for three oxygen concentrations, 1.4, 2.8 and 6.5×10^{13} molecule cm^{-3}, measured with [HAC] $= 1.5 \times 10^{13}$ and $[F]_0 = 5.4 \times 10^{11}$ molecule cm^{-3}. Identical results were obtained by monitoring MGL at *m*/*e* 91 and 109. The k_{2a} value was fitted in calculation using the reaction scheme reported in Table 8. In the scheme, a rate constant typical for F-atoms reaction with small oxygenated molecules (ethanol, acetone, etc.), $k_{14} = 1 \times 10^{-10}$ cm^3 molecule^{-1} s^{-1}, was taken for initiation reaction 14. The sensitivity analysis at $t = 10$ ms showed that MGL concentration is sensitive only to k_2 and k_{14}. In relative measurements of MGL signal intensities, only k_{2a} is responsible for the change of MGL concentration with oxygen. The best fit of the three profiles (solid curves) was obtained with $k_{2a} = 2.8^{+0.8}_{-0.6} \times 10^{-12}$ cm^3 molecule^{-1} s^{-1}. Dashed curves in Figure 5 show the deviation caused by $^{+30}_{-20}$% change of k_2 corresponding to the indicated error limit. For simplicity, the result can be expressed as $k_{2a} = (3.0 \pm 0.6) \times 10^{-12}$ cm^3 molecule^{-1} s^{-1}. The rate constant obtained is lower than that for the H abstraction by O_2 from some carbon-centered hydroxy radicals, e.g., from CH_3CHOH ($k = 1.9 \times 10^{-11}$ cm^3 molecule^{-1} s^{-1}) or from C_2H_5CHOH ($k = 2.6 \times 10^{-11}$ cm^3 molecule^{-1} s^{-1}).[27] Perhaps, the presence of the carbonyl group hinders formation of hydrogen bonding between H-atom of hydroxyl group and O_2.

3.4. Mechanisms of the Secondary Reactions with O_2. Having obtained the yields of nearly all the possible products, we can build the mechanisms of the reactions of the primary radicals from reaction 1 with molecular oxygen. Formation of MGL in reaction 2a by H-atom abstraction is a typical pathway of O_2 interaction with RCHOH radicals producing aldehydes:

$$CH_3C(O)CHOH + O_2 \rightarrow CH_3C(O)CHO + HO_2 \quad (2a)$$

The most intriguing question is formation of equal amounts of formic and acetic acids. Formation of acetic acid *cannot* be explained by OH addition to the carbon of the carbonyl group in HAC followed by elimination of CH_2OH radical, because CH_3COOH is produced in the F + HAC reaction as well. A

possible explanation is the addition of O_2 to the primary radical followed by decomposition of the peroxy adduct:

$$CH_3C(O)CHOH + O_2 \rightarrow [CH_3C(O)CH(OH)OO]$$

$$[CH_3C(O)CH(OH)OO] \rightarrow HCOOH + \text{products} \quad (2b)$$

$$\rightarrow CH_3COOH + \text{products} \quad (2c)$$

The $CH_3C(O)CHOH$ radical can exist in two tautomeric forms:

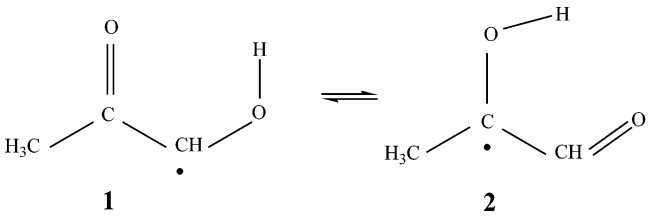

1 **2**

Addition of O_2 to structure **1** can form formic acid in the two following pathways:

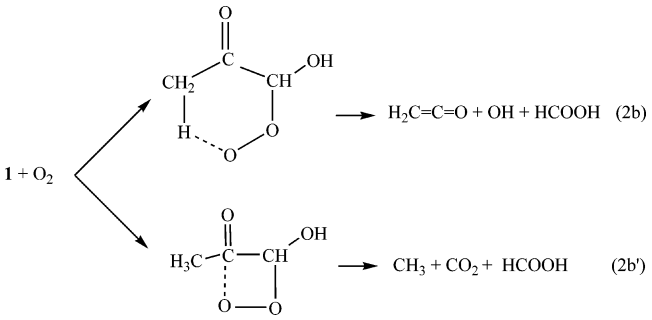

This can occur either through a six-centered transition state with decomposition to CH_2CO, OH and HCOOH (pathway 2b) or through a four-centered transition state with decomposition to CH_3, CO_2 and HCOOH (pathway 2b′). Reaction of the second structure with oxygen leads to formation of acetic acid. In this case, also, two pathways are possible:

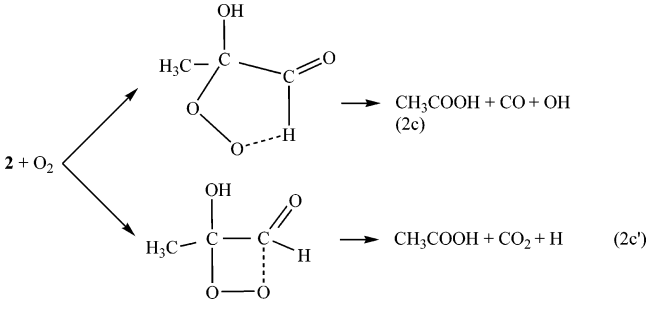

The temperature dependence of the branching ratio of reaction 2 can be explained by the fact that (2a) proceeds by hydrogen abstraction either from structure **1** or from structure **2**, which is more efficient at higher temperature, whereas formation of $R-O_2$ complex by addition to carbon results in the decomposition with elimination of the acid molecule (i.e., lower temperature favoring complex formation and higher temperature favoring abstraction). Indeed, the rate constant of the analogous hydrogen abstraction reaction

$$CH_2OH + O_2 \rightarrow CH_2O + HO_2 \quad (15)$$

decreases with the decrease of temperature ($k_{15} = 8.6 \times 10^{-12}$ and 2.2×10^{-12} cm^3 moleule^{-1} s^{-1} at 300 and 215 K, respectively[28]). In case of reaction 2a, abstraction of the hydroxylic hydrogen by the oxygen molecule is hindered by the intramolecular hydrogen bonding present in the two tautomers. This can explain the lower rate constant of reaction 2a compared to those of O_2 reactions with CH_2OH, CH_3CHOH and C_2H_5CHOH producing aldehyde and HO_2. Decrease of temperature increases the importance of the complexes, leading to enhanced production of formic and acetic acids.

To decide which pathways occur, the yield of CO_2 can be compared to the yields of the acids. The final products of the two minor channels of reaction 1 must first be considered. Channel 1b yields CH_2O and acetylperoxy radicals. The latter can give CO_2 in the reaction with OH, NO (if $H + NO_2$ reaction is used to generate OH radicals), or in its self-reaction:

$$CH_3C(O)OO + OH \rightarrow CH_3 + CO_2 + HO_2 \quad (16)$$

$$CH_3C(O)OO + NO \rightarrow CH_3 + CO_2 + NO_2 \quad (17)$$

$$CH_3C(O)OO + CH_3C(O)OO \rightarrow 2CH_3 + 2CO_2 + O_2 \quad (18)$$

However, OH and, accordingly, NO and $CH_3C(O)OO$ concentrations were always so very low that all these reactions could yield no more than 0.2% of CO_2. The $CH_2C(O)CH_2OH$ radical from (1c) forms an adduct with O_2, which can be stabilized or decompose:

$$CH_2C(O)CH_2OH + O_2 \rightarrow [OOCH_2C(O)CH_2OH]$$

$$[OOCH_2C(O)CH_2OH] \rightarrow OOCH_2C(O)CH_2OH \quad (5a)$$

$$\rightarrow 2CH_2O + CO + OH \quad (5b)$$

$$\rightarrow CH_2CO + CH_2O + HO_2 \quad (5c)$$

$$\rightarrow CH_2O + CO_2 + CH_2OH \quad (5d)$$

The first two decomposition paths (5b) and (5c) can result from the hydrogen bonding of the hydroxyl hydrogen with the terminal attached oxygen; (5b) is about 9 kcal mol^{-1} more exothermic and seems more probable. Moreover, if the yield of formaldehyde from (1b) is equal to the measured yield of the acetylperoxy radicals, about 3%, formation of two CH_2O molecules in reaction 5b well explains the total formaldehyde yield of about 10% if reactions 1b and 1c occur with approximately equal probabilities. In other words, branching fractions of about 3% can be assigned to the two minor channels (1b) and (1c) of the title reaction on the basis of the yields of $CH_3C(O)O_2$ and CH_2O. A CO_2 molecule can be eliminated in (5d). Although this channel is the most energetically profitable decomposition pathway, it should pass through the four-centered transition state corresponding to the interaction of the terminal oxygen with the carbonyl group. In the presence of O_2, the CH_2OH radical will react to give CH_2O and HO_2, suggesting that the CH_2O yield from (5d) is the same as from (5b), i.e., about 7%. Hence, production of CO_2 from the minor channels cannot exceed 3−4% compared to the measured yield of about 12%. It can be concluded that formation of the acids is accompanied, at least partly, by formation of CO_2. From another side, the acids formation can be accompanied by re-formation of OH, as suggested by (2b) and (2c).

3.5. OH Re-formation. The OH re-formation in reaction 1 was examined using the isotope reaction,

$$OD + CH_3C(O)CH_2OH + O_2 \rightarrow \text{products} + HOD + OH \quad (1D)$$

where OD radicals were obtained in the $D + NO_2 \rightarrow OD +$

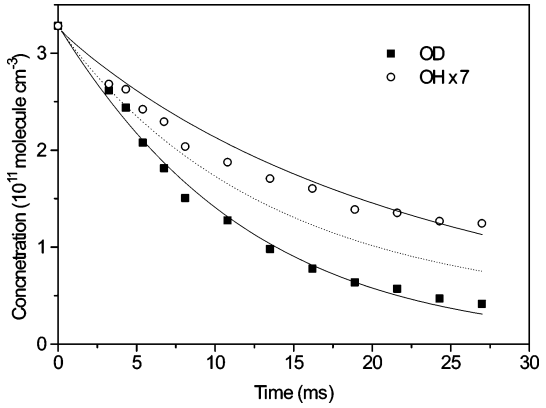

Figure 6. OH re-formation in the OD + HAC reaction (see text).

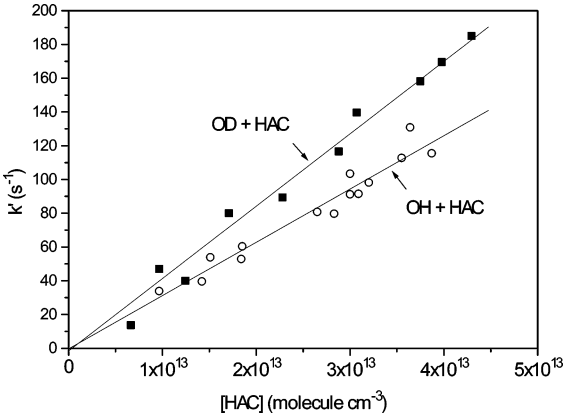

Figure 7. First-order rate constants for the OH (○) and OD (■) reactions with HAC as a function of HAC concentration.

NO reaction. In our study, the kinetics of the OH appearance in reaction 1D is complicated by the presence of OH due to water impurities in the flow through the discharge. Figure 6 shows the OD and OH time profiles measured with initial concentrations $[OD]_0 = 3.3 \times 10^{11}$ and $[OH]_0 = 4.6 \times 10^{10}$ molecule cm^{-3}. Concentrations of HAC and O_2 were 1.2×10^{13} and 1.4×10^{15} molecule cm^{-3}, respectively. In Figure 6, the initial OH concentration is normalized to the initial OD concentration. The different decay kinetics for the two radicals is obvious. Two effects can be responsible for this difference, re-formation of OH and/or a kinetic isotope effect (KIE); i.e., if the rate constant of OH reaction is lower than that of OD reaction, $k_{OH}/k_{OD} < 1$. As a rule, k_{OH}/k_{OD} is close to unity, but noticeable inverse KIEs have been observed for a number of reactions (e.g., OH + acetone, nitric acid, methanethiol[29]). It must be taken into account that, except for the secondary reactions with O_2 (reactions 2b, 2c, 4b and 5b), OH can be reproduced in two secondary reactions taking place in the reactor when NO_2 is used to generate OD:

$$H + NO_2 \rightarrow OH + NO \qquad (7)$$

$$HO_2 + NO \rightarrow OH + NO_2 \qquad (19)$$

Concentration of NO_2 in the reactor corresponds to the nonreacted NO_2 from the injector, about 1×10^{12} molecule cm^{-3}, and H-atoms can be produced in (2c′). Concentration of NO is approximately equal to the initial concentration of OD. Reaction 19 in not important if [NO] is less than 10^{12} molecule cm^{-3}, which is fulfilled in our study. The role of reaction 7 depends on O_2 concentration due to the competing reaction H + O_2 and can be neglected at $[O_2] > 10^{15}$ molecule cm^{-3}.

The KIE was determined by measuring the OD and OH decays in the pseudo-first-order conditions at different HAC concentrations (Figure 7). OH measurements were conducted at low background O_2 concentrations and low OH initial concentrations to minimize the re-formation effects. The rate constants obtained are $k_{OH} = k_1 = (3.17 \pm 0.22) \times 10^{-12}$ and $k_{OD} = k_{1D} = (4.08 \pm 0.31) \times 10^{-12}$ cm^3 molecule^{-1} s^{-1}, giving $k_{OH}/k_{OD} = 0.78 \pm 0.10$. The k_1 value is in good agreement with earlier measurements of $(3.0 \pm 0.5) \times 10^{-12}$.[5,30,31] The dotted curve in Figure 6 shows the calculated OH kinetics corresponding to $k_1 = 3.2 \times 10^{-12}$ cm^3 molecule^{-1} s^{-1}, without OH re-formation reactions, i.e., the difference of the actual OH decay (solid squares), and this curve is the OH reproduction. The solid curves were calculated from the full reaction scheme reported in Table 8. The rate constants for reactions 2b and 2c were assumed to be equal according to the yields of acids. Equal probabilities were also assumed for (5b) and (5d). The fitted values were found to be $k_{2b} = k_{2c} = 1.1 \times 10^{-13}$ cm^3 molecule^{-1} s^{-1}, giving the value of the OH re-formation "yield" of $0.94\text{-}(k_{2b} + k_{2c})/k_2 + 0.03 \cdot k_{4b}/k_4 + 0.03 \cdot k_{5b}/k_5 = 0.082$. Comparison of this fraction of the OH re-formation with the CO_2 yield of 12% suggests an approximate branching between the channels (2b):(2b′) and (2c):(2c′) of about 0.7.

To determine OH re-formation at low temperatures, a simpler analytical method was used. Having obtained k_1 and k_{1D}, we can find an analytical solution for the simplified system of kinetic equations in the pseudo first-order conditions with respect to HAC:

$$\begin{aligned}
OH + HAC &\rightarrow \text{products other than OH} && (1-\beta)\cdot k_1\\
OH + HAC &\rightarrow OH + \text{other products} && \beta \cdot k_1\\
OD + HAC &\rightarrow \text{products other than OH} && (1-\beta)\cdot k_{1D}\\
OD + HAC &\rightarrow OH + \text{other products} && \beta \cdot k_{1D}\\
OH,OD &\rightarrow \text{loss} && k_{loss}
\end{aligned}$$

Here β denotes the branching fraction of all channels producing OH, so that $\beta = \Phi(OH)_{O_2} + \Phi(OH)_{NO_x}$, where these two terms denote OH formation yields in the reactions with O_2 and in reactions 7 and 18, respectively. In our conditions the second term was negligible. The assumption made in writing this kinetic scheme is that the characteristic time of the secondary reactions with O_2 is much smaller than the characteristic time of reaction 1. This can be achieved using sufficiently high O_2 concentration. Hydroxyl radical losses in reactions with NO_2 and NO and wall loss are included in k_{loss}. The solutions of the system are

$$[OD] = [OD]_0 e^{-(k_{1D}\cdot[HAC]+k_{loss})\cdot t}$$

$$[OH] = ([OH]_0 - \gamma\cdot[OD]_0)e^{-((1-\beta)k_1\cdot[HAC]+k_{loss})\cdot t} + [OD]_0 e^{-(k_{1D}\cdot[HAC]+k_{loss})\cdot t}$$

where $\gamma = \beta\cdot\delta/(1 - \beta - \delta)$ and $\delta = k_{1D}/k_1$. The latter expression can be rewritten as

$$\ln\frac{[OH] + \gamma\cdot[OD]}{[OH]_0 + \gamma\cdot[OD]_0} = -\left(\frac{1-\beta}{\delta}\cdot k_{1D}\cdot[HAC] + k_{loss}\right)\cdot t$$

When OH and OD kinetics are measured separately, we can write

$$\ln\frac{[OD]}{[OD]_0} = -(k_{1D}\cdot[HAC] + k_{loss})\cdot t = -p_2\cdot t$$

$$\ln\frac{[OH]}{[OH]_0} = -\left(\frac{1-\beta}{\delta}\cdot k_{1D}\cdot[HAC] + k_{loss}\right)\cdot t = -p_1\cdot t$$

from which follows

$$\beta = \frac{(p_2 - k_{loss}) - \delta\cdot(p_1 - k_{loss})}{p_2 - k_{loss}} = 1 - \delta\cdot\frac{p_1 - k_{loss}}{p_2 - k_{loss}}$$

where p_1, p_2 are respectively the slopes of the plots of ln([OH]/[OH]$_0$), ln([OD]/[OD]$_0$) vs reaction time in the presence of HAC, and k_{loss} the slope of the plots of either ln([OH]/[OH]$_o$) or ln([OD]/[OD]$_o$) vs time in the absence of HAC. An example of such a measurement at 298 K with [HAC] = 1.2×10^{13}, [O_2] = 1.6×10^{15} molecule cm^{-3} and initial concentrations [OH]$_0$ = 3.7×10^{11} and [OD]$_0$ = 3.1×10^{11} molecule cm^{-3} is shown in Figure 8. The star symbols correspond to the decay in the

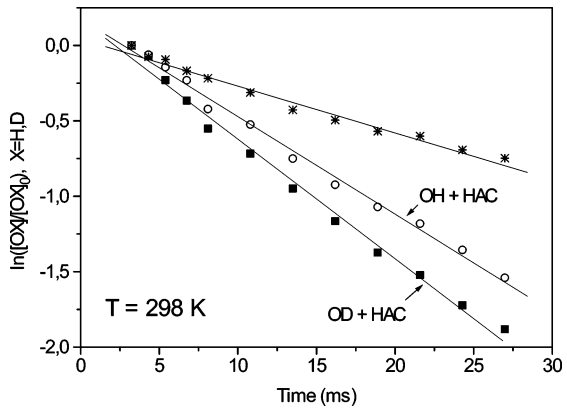

Figure 8. Separate kinetic measurements of OD (■) and OH (○) decay in reaction with HAC. Upper line (∗) corresponds to the OH losses in the absence of HAC.

absence of the reactant, giving the first-order rate constant k_{loss} = 31 s^{-1}. The slopes obtained are given in the upper row of Table 9. The calculated fraction of the reproduced OH is 9.5%, which agrees well with the value from rate constant fitting in the numerical simulation. However, most of the measurements were performed with simultaneous generation of OH and OD. In this case, the expression for β takes the form

$$\beta = \frac{(p_2 - \gamma\cdot p_3) + (\gamma - 1)\cdot k_{loss}}{p_2 - k_{loss}}$$

where p_3 is the slope of the plot of ln{([OH] + γ[OD])/([OH]$_0$ + γ[OD]$_0$)} vs reaction time. Because γ is a function of β, the latter equation was solved numerically by fitting β using the data processing program (EXCEL). Figure 9 presents the OH and OD kinetics in reaction with HAC measured at 298, 253 and 236 K with [HAC] = 1.2×10^{13}, [O_2] = 1.6×10^{15} molecule cm^{-3} and initial concentrations [OH]$_0$ = 3.7×10^{11} and [OD]$_0$ = 3.1×10^{11} molecule cm^{-3}. The slopes and calculated fraction of OH re-formation obtained at different temperatures are given in Table 9. The room-temperature values confirm the previous measurements and give an average value of Φ(OH) = 10.2%. The OH yield increases with the decrease of temperature and reaches 25% at 236 K. This increase correlates with the yields of the acids (see Table 5).

4. Atmospheric Implication

The results obtained revealed that the along with aldehydes (MGL and formaldehyde) formic and acetic acids are produced

TABLE 9: Measurements of the OH Re-formation (in %) in the OH/OD + Hydroxyacetone + O_2 System[a]

T (K)	k_{loss}	p_2	p_3	Φ(OH)
298	30.8 ± 2	79.9 ± 3.1	64.7 ± 2.5[b]	9.5 ± 2.2
	27.2 ± 1	185.5 ± 4.1	134.2 ± 4.5	10.9 ± 2.7
	26.9 ± 2	115.5 ± 2.1	91.2 ± 2.9	10.7 ± 2.5
273	27.2 ± 1	213 ± 9.0	153.3 ± 9.5	13.6 ± 2.6
263	26.9 ± 2	133.3 ± 6.5	97.0 ± 6.4	17.8 ± 4.3
253	30.8 ± 1.9	129.7 ± 1.9	91.4 ± 2.3	20.9 ± 3.3
	27.2 ± 1	258.1 ± 5.5	171.6 ± 6.3	21.7 ± 3.4
236	26.9 ± 1	51.8 ± 5.1	45.0 ± 4.3	24.8 ± 4.4
	27.2 ± 1	223.6 ± 3.6	160.8 ± 8.0	24.5 ± 6.1

[a] k_{loss} is the rate constant of the hydroxyl radical losses in the absence of HAC; p_2 and p_3 are the slopes of the plots of ln([OH] + γ[OD]) and ln([OD]) vs reaction time, respectively (see text for the definition of γ and calculation of Φ(OH)). [b] p_1 value is the slope of ln([OH]) plot, from separate decay measurement.

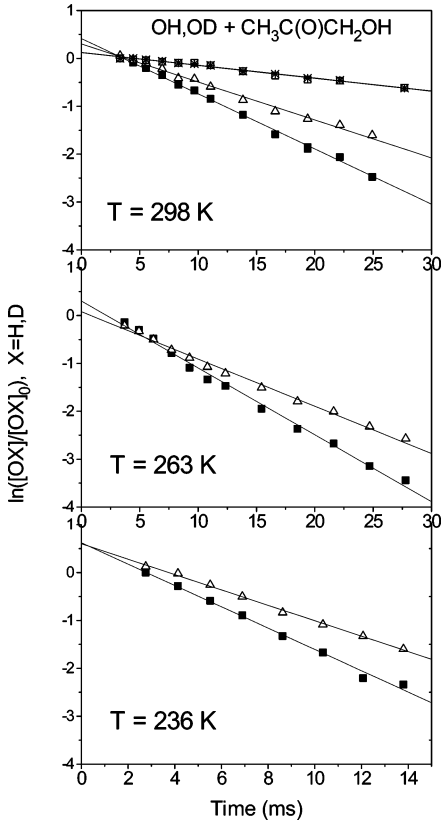

Figure 9. Dependence of ln([OD]/[OD]$_0$) (■) and ln(([OH] + γ[OD])/([OH]$_0$ + γ[OD]$_0$)) (△) on reaction time in the simultaneous OH and OD + HAC reactions. The upper dependences at 298 K for ln([OD]/[OD]$_0$) (□) and ln([OH]/[OH]$_0$) (∗) were measured in the absence of HAC.

in the OH-initiated oxidation of hydroxyacetone (~8% each at T = 298 K). Moreover, the oxidation mechanism changes with temperature: a decrease from 298 to 235 K increases production yields of acids to ~20% each whereas the formation yield of methylglyoxal decreases. These results could have implications regarding the role of isoprene as a potentially significant HO_x precusor in the upper troposphere (UT), because hydroxyacetone is an oxidation product of isoprene. Isoprene can be lifted to the UT by deep vertical convective flows.[3,4] This has been confirmed by a single observation of isoprene by PTR−CIMS at 10−12 km over tropical forest.[32] Rather high concentration values (≈ 1 ppbv) were measured. The use of our results in models would lead to a lower HO_x production rate from isoprene oxidation compared to that calculated from the data available so far only at 298 K. A fraction of methylglyoxal, an efficient

source of HO_x through photolysis, has to be replaced by acids (CH_3COOH and HCOOH), which produce less HO_x by degradation. Another consequence of our results is that the OH-initiated oxidation of isoprene could significantly contribute to CH_3COOH formation observed in the UT (e.g., see refs 33−35). A simple box model calculation including the sequence of reactions of OH with isoprene (a), methacrolein (b), hydroxyacetone (c), and acetic acid (d) with $k_a = 1 \times 10^{-10}$, $k_b = 3 \times 10^{-11}$[1], $k_c = 5 \times 10^{-12}$,[6] and $k_d = 2.2 \times 10^{-12}$ [20] cm^3 $molecule^{-1}$ s^{-1} was carried out. The product yields taken were isoprene → 0.23 methacrolein, methacrolein → 0.45 hydroxyacetone[1] and hydroxyacetone → 0.20 acetic acid (this work). Accounting for a typical residence time in the UT of 15 days, a quasi stationary concentration ratio, acetic acid/isoprene, of about 0.4 was obtained, indicating that isoprene must be considered as a potentially important source of acetic acid in the UT.

Acknowledgment. The work was done in the frames of UTOPIHAN-ACT project of the European Union and the National Program of Atmospheric Chemistry (PNCA) of CNRS.

References and Notes

(1) Carter, W. P. L.; Atkinson, R. *Int. J. Chem. Kinet*. **1996**, *28*, 497.
(2) Orlando, J. J.; Tyndall, G. S.; Paulson, S. E. *Geophys. Res. Lett*. **1999**, *26*, 2191.
(3) von Kuhlmann, R.; Lawrence, M. G.; Pöschl, U.; Crutzen, P. J. *Atmos. Chem. Phys*. **2004**, *4*, 1.
(4) Doherty, R. M.; Stevenson, D. S.; Collins, W. J.; Sanderson, M. G. *Atmos. Chem. Phys. Discuss.* **2005**, *5*, 3747.
(5) Orlando, J. J.; Tyndall, G. S.; Fracheboud, J.-M.; Estupiñan, E. G.; Haberkorn, S.; Zimmer, A. *Atmos. Environ.* **1999**, *33*, 1621.
(6) Hölscher, D.; Dillon, T. J.; Crowley, J. N. *Book of abstracts, 18th International Symposium on Gas Kinetics*; Bristol: U.K., 2004; p 99.
(7) Kwok, E. S. C.; Atkinson, R. *Atmos. Environ.* **1995**, *29*, 1685.
(8) Jenkin, M. E.; Cox, R. A.; Emrich, M.; Moortgat, G. K. *J. Chem. Soc., Faraday Trans*. **1993**, *89*, 2983.
(9) Tyndall, G. S.; Orlando, J. J.; Wallington, T. J.; Hurley, M. D. *Int. J. Chem. Kinet*. **1997**, *29*, 655.
(10) Blitz, M. A.; Heard, D. E.; Pilling, M. J. *Chem. Phys. Lett*. **2002**, *363*, 374.
(11) Kukui, A.; Borissenko, D.; Laverdet, G.; Le Bras, G. *J. Phys. Chem. A* **2003**, *107*, 5732.
(12) Butkovskaya, N. I.; Kukui, A.; Pouvesle, N.; Le Bras, G. *J. Phys. Chem. A* **2005**, *109*, 6509.
(13) Ikezoe, Y.; Matsuoka, S.; Takebe, M.; Viggiano, A. "Gas-phase ion−molecule reaction rate constants through 1986", Ion Reaction Research Group of the Mass Spectrometry Society of Japan, Maruzen Company: Tokyo, 1987.
(14) Elrod, M. J.; Ranschaert, D. L.; Schneider, N. J. *Int. J. Chem. Kinet*. **2001**, *33*, 363.
(15) Butkovskaya, N. I.; Kukui, A.; Le Bras, G. *J. Phys. Chem. A* **2004**, *108*, 1160.
(16) Dotan, I.; Davidson, J. A.; Strait, G. E.; Albritton, D. L.; Fehsenfeld, F. C. *J. Chem. Phys*. **1977**, *67*, 2874.
(17) Midey, A. J.; Arnold, S. T.; Viggiano, A. A. *J. Phys. Chem. A* **2000**, *104*, 2706.
(18) *NIST Chemistry Webbook*; Standard Reference Database 69; NIST: Gaithersburg, MD, 2005.
(19) Mu, Y.; Mellouki, A. *J. Photochem. Photobiol. A* **2000**, *134*, 31.
(20) Butkovskaya, N. I.; Kukui, A.; Pouvesle, N.; Le Bras, G. *J. Phys. Chem. A* **2004**, *108*, 7021.
(21) Hatakeyama, S.; Washida, N.; Akimoto, H. *J. Phys. Chem.* **1986**, *90*, 173.
(22) Yeung, L. Y.; Pennino, M. J.; Miller, A. M.; Elrod, M. J. *J. Phys. Chem. A* **2005**, *109*, 1879.
(23) Boodaghians, R. B.; Hall, I. W.; Toby, F. S.; Wayne, R. P, *J. Chem. Soc., Faraday Trans*. 2 **1987**, *83*, 2073.
(24) Bode, S.; Berces, T.; Temps, F.; Wagner, H. G.; Ziemer, H. *Symp. (Int.) Combust., 25th* **1994**, 775.
(25) Sehested, J.; Christensen, L. K.; Nielsen, O. J.; Wallington, T. J. *Int. J. Chem. Kinet.* **1998**, *30*, 913.
(26) Zhu, L.; Johnston, G. *J. Phys. Chem*. **1995**, *99*, 15114.
(27) *NIST Chemical Kinetics Database*; Standard Reference Database 17, Web Version 7.0, Release 1.3; NIST: Gaithersburg, MD.
(28) Nesbitt, F. L.; Payne, W. A.; Stief, L. J. *J. Phys. Chem*. **1988**, *92*, 4030.
(29) (a) Gierczak, T.; Gilles, M. K.; Bauerle, S.; Ravishankara, A. R. *J. Phys. Chem. A* **2003**, *107*, 5014. (b) Brown, S.; Burkholder, J. B.; Talukdar, R. K.; Ravishankara, A. R. *J. Phys. Chem. A* **2001**, *105*, 1605. (c) Butkovskaya, N. I.; Setser, D. W. *J. Phys. Chem. A* **1999**, *103*, 6921.
(30) Dagaut, P.; Liu, R.; Wallington, T. J.; Kurylo, M. J. *J. Phys. Chem.* **1997**, *93*, 7838.
(31) Chowdhury, P. K.; Upadhyaya, H. P.; Naik, P. D.; Mittal, J. P. *Chem. Phys. Lett*. **2002**, *351*, 201.
(32) Warneke, C.; Holzinger, R.; Hansel, A.; Jordan, A.; Lindinger, W.; Pöschl, U.; Williams, J.; Hoor, P.; Fischer, H.; Crutzen, P. J.; Scheeren, H. A.; Lelieveld, J. *J. Atmos. Chem*. **2001**, *38*, 167.
(33) Jacob, D. J.; Heikes, B. G.; Fan, S.-M.; Logan, J. A.; Mauzerall, D. L.; Bradshaw, J. D.; Singh, H. B.; Gregory, G. L.; Talbot, R. W.; Blake, D. R.; Sachse, G. W. *J. Geophys. Res.* **1996**, *101*, 24235.
(34) Talbot, R. W.; Dibb, J. E.; Lefer, B. L.; Scheuer, E. M.; Bradshaw, J. D.; Sandholm, S. T.; Smyth, S.; Blake, D. R.; Blake, N. J.; Sachse, G. W.; Collins, J. E.; Gregory, G. L. *J. Geophys. Res.* **1997**, *102*, 28303.
(35) Reiner, T.; Möhler O.; Arnold, F. *J. Geophys. Res.* **1999**, *104*, 13943.